Dalton Transactions

Accepted Manuscript

ROYAL SOCIETY OF CHEMISTRY

www.rsc.org/dalton

Dalton Transactions

Cite this: DOI: 10.1039/c0xx00000x

www.rsc.org/dalton

PAPER

A simple BODIPY-aniline-based fluorescent chemosensor as multiple logic operations for the detection of pH and CO_2 gas

Zhong-Hua Pan,[a] Geng-Geng Luo,[a,b*] Jing-Wei Zhou,[c] Jiu-Xu Xia,[b] Kai Fang[b] and Rui-Bo Wu[c]

Received (in XXX, XXX) Xth XXXXXXXXX 2014, Accepted Xth XXXXXXXXX 2014
First published on the web Xth XXXXXXXXX 2014
DOI: 10.1039/b000000x

A simple 4-aniline boron-dipyrromethene (BODIPY) dye (**1**) was developed as a highly sensitive acidic pH fluorescent probe excitable with visible light based on photoinduced electron transfer (PeT) mechanism. The pH titration indicates that the fluorescence intensity increases more than 500-fold within the pH range of 4.12-1.42 with the pK_a value of 3.24 in methanol-water (1:1, v/v) solution, which is valuable for studying strongly acidic conditions. Density functional theory (DFT) calculations reproduce the fluorescence off-on behavior. **1** has also been used as a fluorescent chemosensor for the visual detection of dissolved carbon dioxide (CO_2) gas. The underlying mechanism of the sensing process is rationalized. This probe can be recovered by bubbling nitrogen (N_2) gas into CO_2-treated solutions for over 10 cycles. In addition, two logic gates (OR and INH) have been achieved at the molecular level by changing the initial states of system **1** and chemical inputs.

Introduction

The determination of pH is of great importance because it usually plays a vital role in extensive areas, not only in our daily life and health care, but also in industrial production and environmental protection.[1] The pH glass electrode is by far the most commonly used pH sensor. However, the traditional glass pH electrode suffers from limitations including electrical interference, the presence of acid error and possible damage.[2] By contrast, measurement of pH by fluorescence-based techniques offers a series of advantages such as high sensitivity, nondestructive character, ease of use, real-time visualization, quick response times and the wide range of indicator dyes available. Although new reports on fluorescent pH sensors are continually published, most of them deal with biotechnological applications and thus concern pH sensors for the physiological range.[3] Relatively less attention was paid on the fluorescent probes which are pH sensitive in the lower pH region (pH < 4).[4,5] In fact, since some media such as those found in the human stomach or environmental water are strongly acidic, it is necessary to develop chemosensors for monitoring pH level of these strongly acidic media.

On the other hand, detection and monitoring of dissolved carbon dioxide (CO_2) gas is of fundamental importance in a diverse array of applications ranging from medical diagnosis to environmental monitoring.[6] Hitherto, many approaches have been developed for the detection of CO_2 such as electrochemical assay, GC-MS, and IR spectroscopic techniques.[7] However, these methods are generally expensive, rely on bulky instrumentation, are often intolerant to interferents, and, in some cases, are unsuitable for real-time measurements of gas streams.[8] In contrast, the development of fluorescence-based CO_2 sensing systems has attracted considerable interest lately with a key goal being to establish simple, inexpensive, rapid sensing capabilities, and ability to operate at ambient temperature.[9] Nevertheless, CO_2 detection remains challenging, in part because CO_2 is a relatively inert and colorless gas. Unlike previous optical methods for CO_2 sensing, which rely primarily on the reaction of CO_2 with nitrogen-donating component to form N-CO_2 adducts with the assistance of fluoride or an external base,[10] we describe here another strategy based on the acidic properties of CO_2 without the addition of external bases or fluorides.

Behind fluorescein, rhodamine, and cyanine derivatives, boron-dipyrromethene (BODIPY) fluorescent dyes have been recognized as the promising ones because of their excellent characteristics such as high fluorescence quantum yields, large absorption coefficients, sharp absorption and fluorescence emission spectra.[11] Herein, we report a highly sensitive fluorescent pH probe based on a simple BODIPY-linked aniline (**1**), which shows more than 500-fold enhanced fluorescence when pH is shifted from 4.12 to 1.42. The mechanism of the sensor to monitor H^+ is based on the reductive photoinduced electron transfer (PeT), which is rationalized by DFT calculations. Probe **1** can also act as a CO_2 fluorescent

[a] *College of Materials Science and Engineering, Huaqiao University, Xiamen 361021, P. R. China*; *E-mail: ggluo@hqu.edu.cn; Fax: 86-592-6162225.*
[b] *State Key Laboratory of Structural Chemistry, Fujian Institute of Research on the Structure of Matter, Chinese Academy of Science, Fuzhou, Fujian 350002, P. R. China*
[c] *School of Pharmaceutical Sciences, East Campus, Sun Yat-sen University, Guangzhou 510006, P. R. China*
† Electronic Supplementary Information (ESI) available: CCDC reference numbers 984559-984561. For ESI and crystallographic data in CIF or other electronic format see DOI:10.1039/b000000x.

chemosensor when dissolved in the CH_3OH/H_2O solution. Furthermore, two molecular level logic operations (OR and INH) based on this "off-on"-type fluorescence sensor could be mimicked by selecting the initial states and chemical inputs.

Experimental

Materials and Apparatus

Unless otherwise noted, reagents of the best available grade were purchased from commercial suppliers and used without further purification. Air- and moisture-sensitive reactions were carried out under a nitrogen atmosphere using oven-dried glassware. Dichloromethane was distilled over calcium hydride. Triethylamine was obtained by simple distillation. Flash column chromatography was performed with silica gel (200-300 meshes) with the eluent reported in parentheses. Analytical thin-layer chromatography (TLC) was performed on precoated glass plates and visualized by UV.

^1H and ^{13}C NMR spectra were recorded in $CDCl_3$ on a Bruker PLUS 400 or 600 MHz spectrometer. All chemical shifts are referenced to Me_4Si (TMS). Chemical shift multiplicities are reported as s = singlet, d = doublet, and br = broad singlet. Coupling constants (*J*) values are given in Hz. Mass spectrometry (MS) experiment was carried out in the positive ion made on a Bruker Esquire HCT ion trap mass spectrometer (Billerica, MA) coupled with a homemade electrospray ionization (ESI) device. Parameters of the ESI source were optimized to enhance the signal intensity. FT-IR spectrum was recorded from KBr pellet in the range 4000-400 cm^{-1} on a Nicolet AVATAT FT-IR360 spectrometer. Cyclic voltammetry was performed on a CHI-660E electrochemical workstation. A standard three-electrode cell at a scan rate of 100 mV s^{-1} was used for the measurement: a Pt wire as the auxiliary electrode, a Pt electrode as the working electrode, and a Ag/Ag^+ electrode as the reference electrode. The sample solution contained 0.1 M tetrabutylammonium hexafluorophosphate ($TBAPF_6$) as the supporting electrolyte. All solutions were purged with nitrogen prior to measurement. Concentrations of analytes were 1mM. A Denver UB-7 digital pH meter was employed to make the pH measurements.

Spectroscopic measurements and determination of quantum yields

BODIPY dye was dissolved in various solvents to acquire optical measurements. Acetonitrile, methanol, tetrahydrofuran, dichloromethane and toluene were all individually used in preparing a BODIPY solution. UV-vis absorption and emission measurements are obtained using a UV-2100 (Shimadzu) spectrophotometer and a F-7000 (Hitachi) spectrophotometer. The slit width was 5 nm for both excitation and emission. Samples for absorption and emission measurements were contained in 1 cm × 1 cm quartz cuvettes.

For the determination of the relative fluorescence quantum yields (Φ_{fl}^{sample}), only dilute solutions with an absorbance below 0.1 at the excitation wavelength λ_{ex} were used. The Φ_{fl}^{sample} values were calculated using synthesized 8-phenyl-4,4-difluoro-1,3,5,7-tetramethyl 4-bora-3a,4a-diaza-*s*-indacene (compound **3**, $\Phi_{fl}^{standard}$ = 0.72 in tetrahydrofuran)[12] or Rhodamine 6G ($\Phi_{fl}^{standard}$ = 0.95 in ethanol)[13] as fluorescence standard using the expression (1) below,

$$\Phi_{fl}^{sample} = \Phi_{fl}^{standard} \times (I^{sample}/I^{standard}) \times (A^{standard}/A^{sample}) \times (n^{sample}/n^{standard})^2 \quad (1)$$

Where Φ_{fl}^{sample} and $\Phi_{fl}^{standard}$ are the emission quantum yields of the sample and the reference, respectively, $A^{standard}$ and A^{sample} are the measured absorbances of the reference and sample at the excitation wavelength, respectively, $I^{standard}$ and I^{sample} are the integrated emission intensities of the reference and sample, respectively, and $n^{standard}$ and n^{sample} are the refractive indices of the solvents of the reference and sample, respectively. The Φ_{fl}^{sample} values reported in this work are the averages of multiple (generally three), fully independent measurements.

Synthetic procedures

The syntheses of BODIPY compounds **1** and **2** were achieved using literature methods.[14]

8-(4-nitro-phenyl)-4,4-difluoro-1,3,5,7-tetramethyl 4-bora-3a,4a-diaza-*s*-indacene (2):

2,4-dimethylpyrrole (380 mg, 4 mmol) and 4-nitro-benzaldehyde (306 mg, 2 mmol) were dissolved in dry CH_2Cl_2 (50 mL) under nitrogen. One drop of trifluoroacetic acid (TFA) was added, and the solution was stirred overnight at ambient temperature in the dark until TLC indicated complete consumption of the aldehyde. Dichlorodicyanobenzoquinone (DDQ, 442 mg, 2 mmol) in dry dichloromethane (20 mL) was added, and the mixture was stirred for additional 30 min. The reaction mixture was then treated with triethylamine (3 mL) and stirring was continued for a further 5 min. Boron trifluoride etherate (3 mL) was added and stirred for another 3h. The mixture was diluted with water (3×20 mL) and extracted with dichloromethane (3×20 mL). The combined organic phase was dried over anhydrous Na_2SO_4 and filtered. The solvent was removed under reduced pressure and the resulting residue was purified via flash column chromatography on silica using hexane/dichloromethane (2:1) as the eluent to deliver 310 mg (45%) of compound **2** as a red solid. ^1H NMR (400 MHz, $CDCl_3$) δ 1.37 (s, 6H), 2.57 (s, 6H), 6.03 (s, 2H), 7.54 (d, 2H, *J* = 8.8 Hz), 8.39 (d, 2H, *J* = 8.8 Hz); ^{13}C NMR (100 MHz, $CDCl_3$) δ 14.5, 121.7, 124.4, 129.6, 130.6, 138.3, 141.9, 142.5, 148.4, 156.3.

8-(4-amino-phenyl)-4,4-difluoro-1,3,5,7-tetramethyl 4-bora-3a,4a-diaza-*s*-indacene (1):

To a stirred solution of **2** (185 mg, 0.5 mmol) in ethanol (30 mL) under nitrogen atmosphere was added 10 mg palladium-carbon (Pd/C) catalyst and 0.7 mL hydrazine. The reaction mixture was stirred at reflux for 5 h until TLC monitoring indicated complete consumption of the starting material. Then the reaction mixture was cooled to room temperature, filtered and concentrated at reduced pressure. The resulting residue was purified via flash column chromatography on silica gel with hexane/dichloromethane (1:2) as the eluent to yield 103 mg (80%) of the title compound **1**. ν_{max}(KBr pellet)/cm^{-1}: 3460, 3370, 1621, 1546, 1507, 1468, 1405, 1374, 1303, 1280, 1255, 1194, 1155, 1101, 990, 827, 764 and 709; ^1H NMR (400 MHz, $CDCl_3$) δ 1.51 (s, 6H), 2.57 (s, 6H), 4.44 (br, 2H), 5.99 (s, 2H), 6.86 (d, 2H, *J* = 4.0 Hz), 7.05 (d, 2H, *J* = 6.8 Hz); ^{13}C NMR (150 MHz, $CDCl_3$) δ 14.5, 14.6, 115.5, 119.7, 120.9, 124.7, 128.8, 128.9, 132.0, 142.6, 143.2, 146.9, 154.9. ESI-MS *m/z* ($C_{19}H_{20}BF_2N_3$) calculated: 339.2, found: 320.3 (M-F).

8-phenyl-4,4-difluoro-1,3,5,7-tetramethyl 4-bora-3a,4a-diaza-*s*-indacene (**3**) was synthesized according to the literature

reports.[15] ^{1}H NMR (400 MHz, $CDCl_3$) δ 1.39 (s, 6H, CH3), 2.58 (s, 6H, CH3), 6.00 (s, 2H), 7.28-7.32 (m, 2H, phenyl), 7.49-7.50 (m, 3H, phenyl); ^{13}C NMR (100 MHz, $CDCl_3$) δ 14.3, 14.6, 121.2, 127.9, 128.9, 129.1, 131.4, 135.0, 141.7, 143.1, 155.4. Since **3** is one of our internal reference dyes it is regularly checked for stability and purity.

Measurements of pH

For every step of the pH titration of neat **1** in solution, a few microliters of aq. HCl (0.01-1 M) were added to a solution containing the dye in a mixed solvent of H_2O and MeOH 1:1 (v/v). The mixture was stirred and the pH value was monitored with a digital pH meter. Calibration of the instruments was performed with standard aqueous solutions of pH 1.68, 4.01 and 7.00. The measurement uncertainties of the pH electrode amount to ≦±0.01 pH.

The acidity constant K_a of probe **1** was determined in methanol/water (1:1, v/v) solution by fluorimetric titration as a function of pH using the fluorescence emission spectrum. Sigmoidal curve fitting of the Henderson-Hasselbalch equation[16] (2) to the fluorescence data recorded as a function of pH yielded values of K_a, the fluorescence intensity FI_{min} and FI_{max} at minimal and maximal [H^+], respectively.

$$pK_a = pH - \log(FI-FI_{max})/(FI_{min}-FI) \quad (2)$$

CO_2 gas sensing experiments

In a typical run, **1** dissolved in a mixed solvent of H_2O and MeOH 1:1 (v/v) with a concentration of ~23 μM was used. CO_2 gas was bubbled into the solution through a 0.5 mm needle. The bubbling rate fixed at 20 mL min^{-1} and the gas volume was controlled by using a gas flowmeter.

Titration experiments were conducted by measuring the changes in fluorescence emission that occurred upon addition of several amines to the CO_2-treated **1** solution.

Crystallization experiments

The quality of single crystals depends on the purity of the used material. Hence, the synthesized BODIPYs were highly purified dyes. All crystallization experiments were carried out under nearly identical conditions. Vials containing solutions of the compound were covered with parafilm and allowed to crystallize and evaporate under ambient conditions in a fume hood. Fast evaporation from hot mix solvents of CH_2Cl_2 and n-hexane (v/v, 3:1) afforded orange crystals of **1**•CH_2Cl_2. Slow crystallization from toluene or acetonitrile yielded another deep red crystals of **1**. It is worth noting that better quality crystals of **1** can be grown toluene than acetonitrile. Suitable crystals of **3** were obtained by the slow evaporation of a solution in CH_2Cl_2/n-hexane (v/v, 1:3) or by slow diffusion of n-hexane into the CH_2Cl_2 solution of **3**.

X-ray crystallography

Intensity data for **1**•CH_2Cl_2, **1** and **3** were collected on a Rigaku R-AXIS RAPID Image Plate single-crystal diffractometer using graphite-monochromated Mo Kα radiation source (λ = 0.71073 Å). Single crystals of **1**•CH_2Cl_2, **1** and **3** with appropriate dimensions were chosen under an optical microscope and mounted on a glass fiber for data collection at low temperature (173 ± 2K). Absorption correction was applied by correction of symmetry-equivalent reflections using the ABSCOR program.[17] All structures were solved by direct methods using SHELXS-97[18] and refined by full-matrix least-squares on F^2 using SHELXL-97[19] via the program interface X-Seed.[20] Non-hydrogen atoms were refined anisotropically and H atoms isotropically in a riding model with U_{iso} values 1.2-1.5 times those of their parent atoms. They all were visible on difference electron density maps. All structures were examined using the Addsym subroutine PLATON[21] to ensure that no additional symmetry could be applied to the models. Crystal structure views were obtained using Diamond v3.1.[22] CCDC reference numbers 984559-984561 for three BODIPY compounds. Some crystallographic data are summarized in Table S1 (ESI†). Selected bond lengths and angles are listed in Table S2 (ESI†).

Hirshfeld surface analyses

Molecular Hirshfeld surfaces in the crystal structure and the associated 2D-fingerprint plots were calculated using *CrystalExplorer* 3.0 program,[23] which accepts a structure input file in CIF format. Bond lengths to hydrogen atoms were set to typical neutron values (C-H = 1.083 Å, N-H = 1.009 Å).[24] For each point on that isosurface two distances are defined: d_e, the distance from the point to the nearest nucleus external to the surface, and d_i, the distance to the nearest nucleus internal to the surface. The normalized contact distance (d_{norm})[23a] based on d_e and d_i is given by:

$$d_{norm} = (d_i - r_i^{vdw})/r_i^{vdw} + (d_e - r_e^{vdw})/r_e^{vdw}$$

Where r_i^{vdw} and r_e^{vdw} are the van der Waals radii of the atoms. The value of d_{norm} is negative or positive depending on whether the intermolecular contacts are shorter or longer than the van der Waals separations. The parameter d_{norm} defines a surface with a red-white-blue color scheme, where red highlights shorter contacts, white is used for contacts around the van der Waals separation, and blue is for longer contacts. Hirshfeld surface fingerprint plots were generated using d_i and d_e as a pair of coordinates, in intervals of 0.01 Å, for each individual surface spot resulting in two-dimensional histograms.

Computational details

For the purpose of accordance with experiment results, the molecular structures of **1** and **3** are taken from the crystal structures before optimization. Geometry optimizations were carried out using density functional theory (DFT) as implemented in Gaussian 03, revision E.01.[25] Becke's three-parameter hybrid functional[26] with the LYP correlation functional[27] (B3LYP) was used with the 6-31g(d) basis set for geometry optimization. Single point energy calculations for the neutral form **1**, the protonated species **1**-H^+ with positive charge and **3** were performed at the B3LYP/6-31G+(d) basis set. The Berny algorithm using redundant internal coordinates[28] was employed and the default cutoffs were used throughout. Vibration frequency calculations were carried out to make sure that the optimized structures were true energy minimum. All molecular orbital contours were plotted using the software Gauss view 5.0.9. The excited-state related calculations (UV-vis absorptions) were carried out with the time-dependent DFT (TDDFT) with the optimized structure of the ground state.

Result and discussion

Synthesis and crystal structures

The BODIPY-linked aniline **1** was synthesized through a reaction of 2,4-dimethylpyrrole and 4-nitro-benzaldehyde followed by a conversion of the $-NO_2$ group to form an $-NH_2$ substituent. **1** was characterized by IR, ^{1}H NMR, ^{13}C NMR and

X-ray crystallography. Two sharp bands at 3370 and 3460 cm^{-1} and one band at 1621 cm^{-1} in solid-state IR spectrum correspond to NH_2 stretching and asymmetric bending vibration (Fig. S1 of ESI†), revealing the presence of amino group in **1**. Recently, we reported discovery of concomitant polymorphism of BODIPY dyes.[29] In the course of searching for polymorphs of BODIPY, we found fast crystallization of **1** from a hot CH_2Cl_2-hexane solution gives orange crystals of **1**•CH_2Cl_2. The orange crystals of **1**•CH_2Cl_2 is relatively unstable and can be transformed into deep red crystals of **1** upon the loss of CH_2Cl_2. Upon exposure of the desolvated sample of **1** to CH_2Cl_2 vapor atmosphere at room temperature, the determination of the unit cell parameters by single-crystal X-ray diffraction analysis (SCXRD) indicated that there was no solvation process or transformation occurring in **1**. These desolvation and solvation experiments indicate that **1** is both thermodynamically and kinetically favored compared with **1**•CH_2Cl_2. It should be noteworthy that the deep red crystals of **1** can also be crystallized by slow evaporation from toluene or slow diffusion of n-hexane into the CH_2Cl_2 solution of **1**.

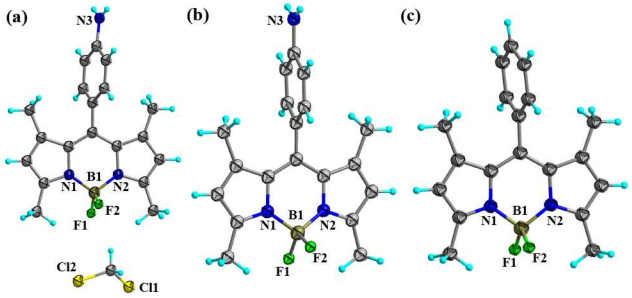

Fig 1 Single crystal X-ray diffraction structures of **1**•CH_2Cl_2 (a), **1** (b) and **3** (c) with thermal ellipsoids set at 50% probability.

In order to facilitate structural comparison, the molecular structure of reference dye **3** was also illustrated by SCXRD. Fig. 1 shows the X-ray crystal structures of **1**•CH_2Cl_2, **1** and **3**. **1**•CH_2Cl_2 is found to crystallize with one dichloromethane solvent molecule in the triclinic space group $P\bar{1}$. **1** crystallizes in the monoclinic space group $P2_1/n$, which is the same to that of **3**. It should be noteworthy that the crystal structure of the deep red species **1** was recently reported, but without any detailed description of molecular packing mode.[30] There is an interesting change in the unit cell parameters upon the removal of one CH_2Cl_2 molecule (Table S1 of ESI†). The shorter *a*-axis expands, while the long *b*- and *c*-axes almost remain unchanged. The cell volume decreases by 15.4%. The C_9BN_2 (BODIPY) framework consisting of one central six-membered and two adjacent five-membered rings is essentially flat, with the maximum deviation from the least-squares mean plan being 0.0259 Å in **1**•CH_2Cl_2, 0.0654 Å in **1**, and 0.0211 Å in **3**, respectively. The introduction of two methyl groups at C-1 and C-7 positions of BODIPY core in **1**•CH_2Cl_2, **1** and **3** were revealed to prevent the free rotation of the benzene moiety, resulting in almost orthogonal configuration between the BODIPY and benzene moiety. The dihedral angle between the *meso*-phenyl ring and the indacene plane (85.8°) in **1** is close to the corresponding value in **3** (85.7 °) but is bigger than that in **1**•CH_2Cl_2 (73.0°), which may be caused by the presence of CH_2Cl_2 solvent. Analysis of the crystal packing diagram of **1**•CH_2Cl_2 reveals the molecules of **1** are packed parallel to each other with head-to-head orientation, leading to a void and CH_2Cl_2 molecule was found to reside within the void through a series of weak hydrogen bonds including C-H···Cl, C-H···F and C-H···π interactions (Fig. S2 of ESI†), but no large cavities were observed in the crystal structure. When **1**•CH_2Cl_2 was transformed into **1**, crystallographic data proved that no solvent molecules were included in the crystals of the desolvated **1** (Fig. S2 of ESI†).

Hirshfeld surface plots and 2D fingerprint analyses provide additional insight into the molecular interactions in these BODIPY derivatives. For the visualization, we have used a mapping of the normalized contact distance, d_{norm}. Its negative value enables identification of molecular regions of great importance for intermolecular interactions. These F- and C-based interactions represent the closest contacts in the structure and can be viewed as a pair of red spots on the d_{norm} surface (Fig. S3 of ESI†). Remarkable differences of intermolecular contacts between **1**•CH_2Cl_2 and **1** can be seen by inspecting H···H and H···Cl regions. H···H contacts comprise 63.2% of the surface area in **1**, and only 53% of the surface in **1**•CH_2Cl_2. Only H···Cl contacts comprising 9.2% are found in **1**•CH_2Cl_2 (Table S3).

Table 1 The spectroscopic data of **1** in various solvents at 298 K.[a,b,c]

Solvent	λ_{abs} (max/nm)	$\log(\varepsilon_{max})$	λ_{em} (max/nm)	λ_{ex} (max/nm)	$\Delta\upsilon_{max}$ (cm^{-1})	Φ_{fl}
MeOH	497	4.89	512	504	589	0.003(0.004)
CH_3CN	496	4.90	508	499	476	0.004(0.01)
THF	500	4.93	512	501	469	0.12(0.06)
CH_2Cl_2	500	4.91	512	502	469	0.30(0.39)
Toluene	502	4.94	515	505	503	0.60(0.66)

[a]$\log(\varepsilon/mol^{-1}\cdot dm^3\cdot cm^{-1})$-molar extinction coefficient, λ_{abs}(absorption maxima), λ_{em}(emission maxima), λ_{ex} (excitation maxima); $\Delta\upsilon_{max}$ (cm^{-1}) = $(1/\lambda_{abs} - 1/\lambda_{em})\times10^7$

[b]8-phenyl-4,4-difluoro-1,3,5,7-tetramethyl 4-bora-3a,4a-diaza-*s*-indacene (**3**) was used as a standard ($\Phi_{fl}^{standard}$ = 0.72 in tetrahydrofuran).[12]

[c]Rhodamine 6G was used as a standard ($\Phi_{fl}^{standard}$ = 0.95 in EtOH)[13] and the calculated Φ_{fl} was listed in parentheses.

Steady-state absorption and emission properties

The electronic absorption and steady-state fluorescence spectra of **1** were first measured in various solvents with increasing polarity from toluene to methanol (Fig. S4 of ESI†), and the data are summarized in Table 1. The electronic absorption maxima of **1** are centered at 500 ± 2 nm, ascribed to the $S_0\rightarrow S_1$ (π-π^*) transition of BODIPY moiety, along with high molar absorption coefficients. The simulated stick spectra of **1** obtained from time-dependent DFT (TDDFT) calculations are consistent with the experimental absorption spectra (Fig. S5 of ESI†). The fluorescence emission spectra display a slightly Stokes-shifted (*ca*. 12 nm), mirror-symmetrical band relative to the absorption of BODIPY unit. The fluorescence excitation spectra closely match the absorption spectra. Moreover, the fluorescent band was hypsochromically shifted and quantum yields were decreased with an increase in the polarity of the solvent. These observations were in agreement with the general behavior of other BODIPYs.[31] The photoluminescence (PL) spectrum of **1** solution in methanol or acetonitrile is nearly a flat line parallel to the abscissa, with a fluorescence quantum yield determined as Φ_{fl} < 1%. This rather low value points to a highly efficient fluorescence quenching by a thermodynamically allowed photoinduced electron transfer (PeT) from the phenylamino unit

to the singlet excited state of the BODIPY moiety. The estimation of free energy change (ΔG_{PeT}) with well-known Rehm-Weller equation ($\Delta G_{PeT} = E_{ox}(D) - E_{red}(A) - E_{00} + C$)[32] yielded exergonic thermodynamics for the excited singlet state process (ΔG_{PeT} = ~ -0.32 eV, with $E_{ox}(D)$ = 0.61 V, $E_{red}(A)$ = -1.55 V and E_{00} = 2.46 eV).[14]

pH-dependent absorption and fluorescence spectroscopy

As mentioned above, the *meso*-phenylamine moiety of **1** is sensitive to the environmental pH and can be protonated to the cation in acid media. The effect of pH was assessed by altering the solution pH from 6.99 to 1.42 through successive addition of aq. HCl in methanol-water (1:1). The spectrophotometric and fluorometric pH titration spectra shown in Fig. 2 reveal that the wavelength of the emission maximum remains unchanged, despite the strong signal increase. In addition, the absorption maximum was shifted to longer wavelengths, in agreement with the influence that a change in inductive effect exerts on the HOMO/LUMO of the BODIPY when converting a into moiety (Fig. 4). The dynamic sensing range spans 3 pH units, 1.42-4.12. The fluorescence intensity in low pH (1.42) was *ca*. 505-fold larger than that in high pH (6.99) for probe **1**. The protonation constant K_a of **1** was determined in methanol/water (1:1, v/v) solution by fluorimetric titration as a function of pH. The analysis of fluorescence intensity changes as a function of pH by using the Henderson-Hasselbalch equation[16]: $-\log[(FI_{max} - FI)/(FI-FI_{min}) = pH - pK_a$ where FI is the observed fluorescence intensity at a fixed wavelength, FI_{max} and FI_{min} are the corresponding maximum and minimum, respectively, yielded a pK_a of 3.24, which is valuable for studying the strong acid pH scale. The acidity dependent on/off fluorescent properties of **1** has enabled the potential use of **1** as an efficient pH-sensitive fluorescent sensor for the acidic pH range.

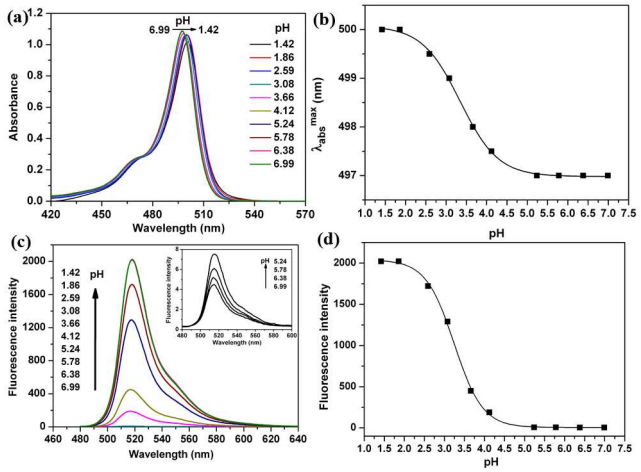

Fig 2 Dependence of the absorption (a) and fluorescence (c) of **1** on a change in pH from 6.99-1.42 upon addition of aq. HCl solution (λ_{ex} = 470 nm, c_1 = 1.3 ×10^{-5} M, MeOH-H_2O V:V = 1:1). The corresponding titration curves were shown when plotting the shift of the absorption maximum (b) and fluorescence intensity at the emission maximum (d) as a function of pH.

To gain insight into the interesting pH-dependent fluorescence characteristics of **1** at molecular and electronic levels, ab initio calculations were carried out on the neutral form **1** and protonated state **1**-H^+ using the Gaussian 03 program with DFT, the B3LYP method, and 6-31+G(d) as the basis set. As shown in Fig. 3, the highest occupied molecular orbital (HOMO) of the phenylamine moiety (electron donor) matches that of the fluorophore BODIPY (electron acceptor); the HOMO energy level (-5.38 eV) of phenylamine moiety is higher than that of the fluorophore BODIPY (-5.78 eV). Consequently, when the BODIPY moiety is photoexcited, the intramolecular electron transfer from the phenylamine moiety to the BODIPY moiety is energetically favorable. Hence the fluorescence of the BODIPY moiety is quenched through a PeT process (Φ < 0.01). In contrast, once **1** is protonated to form **1**-H^+ in acidic solutions, the HOMO energy level of phenylammonium moiety (-8.09 eV) is obviously lower than that of the BODIPY unit; therefore, the PeT process is restricted and the fluorescence BODIPY is restored.

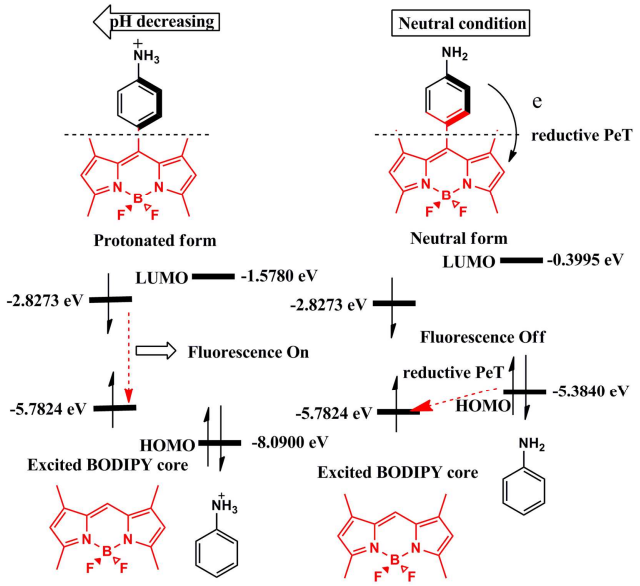

Fig 3 Proposed photoinduced electron transfer (PeT) mechanism between BODIPY moiety and phenylamino unit of **1** in protonated and neutral form, respectively.

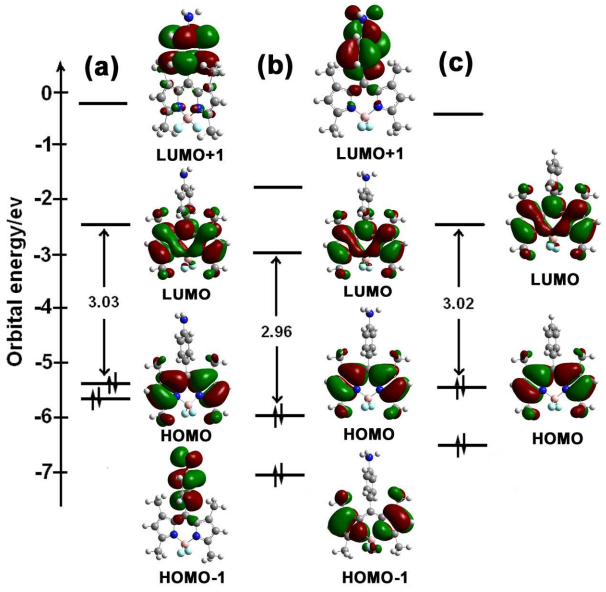

Fig 4 Energy levels and surfaces of frontier MOs of (a) **1**, (b) **1**-H^+ and (c) an reference dye **3** calculated at the B3LYP/6-31+G(d) levels.

In addition, according to the DFT calculations, the HOMO-1 and LUMO orbitals of **1** are localized on the phenylamino moiety and BODIPY moiety, respectively, as shown in Fig. 4. However, both the contours of the electronic distribution in HOMO and LUMO states of **1**-H^+ are located almost completely on the BODIPY moiety, while LUMO+1 state is located mainly on the phenylamine unit. It is postulated that the HOMO-LUMO transition corresponds to the emissive π-π* excited state as observed in the reference dye **3** (Fig. 4) and other BODIPY derivatives.[11] As a result, the electronic transition between HOMO and LUMO for **1**-H^+ limited only on the BODIPY moiety leads to an intensive intrinsic fluorescence from the BODIPY moiety of **1**-H^+.

As far as we know, some fluorescent pH probes based on quenching of BODIPY fluorophore by linking amines have been reported,[33] which are representatives of orthogonal 'fluor-spacer-receptor' format with C_1 skeletons as common spacers. The probe **1** is also considered as orthogonal 'fluor-spacer-receptor' assembly with a virtual C_0 spacer based on the structure analysis. Besides the structural difference, **1** as fluorescent pH sensor has the following several prominent advantages: (1) Probe **1** can be used to detect strongly acidity within pH range 1.42-4.12 with the pK_a value of 3.24. (2) Compared to the reported systems only showing less than 20-fold fluorescence enhancement, system **1** is the most sensitive fluorescent probe at acidic pH (the result of protonation boosted its emission efficiency by as much as 500 times). (3) This probe can be readily synthesized in two steps from commercially available chemicals.

1 chosen as fluorescent chemosensor for detection of CO_2

CO_2 sensing is of great societal implications, as CO_2 is a component of gas mixtures from many natural and anthropogenic processes with huge impacts on globe climate and human well-being. **1** has been used as a fluorescent chemosensor for dissolved carbon dioxide gas. Fluorescence emission centered at 518 nm of **1** was intensified with increasing the volume of CO_2 gas. After being bubbled with 10 mL of CO_2 gas, the mixture was saturated and emitted a very bright green light, and no additional changes in the emission features were observed. The saturation curve is shown in the inset of Fig. 5a, which also provides a representative plot of the fluorescence intensity (I_{518nm}) of a solution of **1** in MeOH/H_2O versus the volume of CO_2 bubbled through the solution. These results confirmed that **1** could be a useful probe for rapid CO_2 sensing. There may be two possible proposed mechanisms for this sensing process: (i) reaction of the tethered phenylamino of **1** with CO_2 to form carbamic acid;[10] (ii) **1** reacts with the proton generated by the hydration of CO_2 to carbonic acid, and to form a protonated species phenylammonium.[34]

CO_2 is a relatively weak electrophile and the phenylamino moiety is a weakly nucleophilic nitrogen-donating component, which suggests mechanism I is a less favored pathway. To obtain insight into the underlying mechanism of the CO_2 sensing process, additional control experiments were carried out. After bubbling with a large volume of CO_2 gas into a solution of **1** in MeOH or CH_3CN, no fluorescence enhancement was observed in the absence of water. These results are easily interpreted in terms of the formation of carbonic acid when CO_2 dissolves in water. Carbonic acid is a weak acid and interacted with phenylamino moiety of **1** to form amounts of phenylammonium that prevent the expected PeT quenching process. To provide support for this supposition, the mass spectrum analyzed by electrospray ionization mass spectrometry (ESI-MS) for CO_2-treated **1** solution was carried out on a Bruker Esquire HCT ion trap mass spectrometer. The ESI-MS predominately shows the protonated species of **1** (*m*/*z* 340.3, see Fig. S6 of ESI†). The above experimental findings were found to be in accord with the mechanism II.

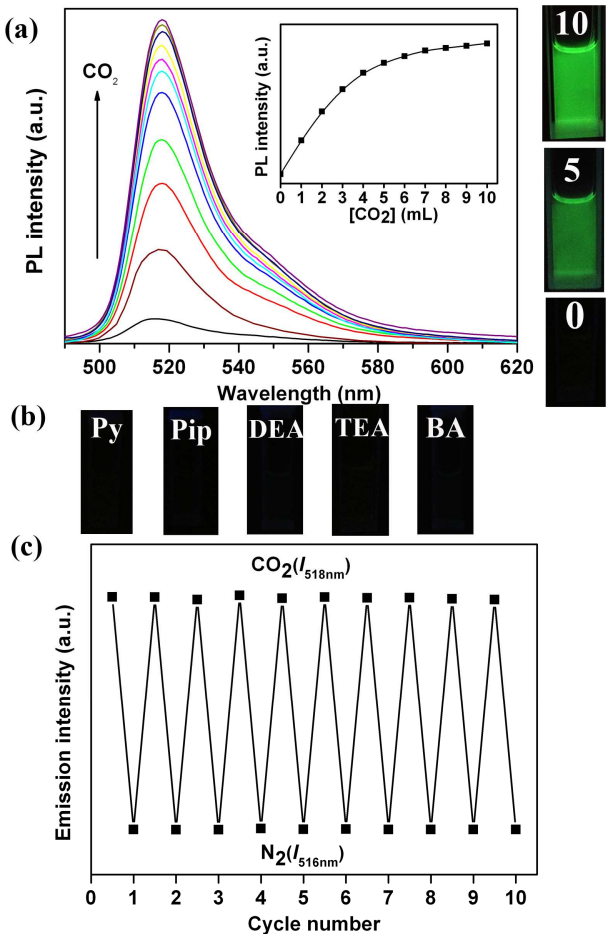

Fig 5 (a) PL spectra and photographs of **1** solution (~23 μM, MeOH/H_2O, v:v = 1:1) after bubbling with different volumes of CO_2, excitation wavelength, 470 nm, slit widths, 5/5 nm. (b) Photographs of CO_2-treated **1** in the amines bubbled with CO_2 gas; Py = pyridine, Pip = piperidine, DEA = diethylamine, TEA = triethyl amine, BA = butylamine. (c) Relative emission intensity of **1** (~23 μM) upon alternating CO_2 and N_2 stimuli. All the photographs were taken under UV illumination.

It is noteworthy that the fluorescence intensity of the CO_2-treated **1** solution was found to be noticeably decreased upon the subsequent addition of triethyl amine (TEA). We screened a series of amines including pyridine (Py), piperidine (Pip), diethylamine (DEA) and butylamine (BA). Unfortunately, bubbling large volumes of CO_2 gas through **1** solution in Py, Pip, DEA and BA caused no recognizable changes in the emission of **1** (Fig. 5b). One possible mechanism for this process is given: when added into the system of CO_2-treated **1**, amines interact with the protonated species **1**-H^+ and deprotonate **1**-H^+ to generate its neutral form **1** in the presence of water according to

the sequence of reactions ($NR_3 + H_2O \leftrightarrow NR_3H^+ + OH^-$; **1**-$H^+$ + $OH^- \leftrightarrow H_2O$ + **1**).[35] The fluorescence of the system is quenched because the emission intensity of the neutral form **1** is obviously weaker compared to that in its protonated form **1**-H^+.

It is known that the gas-liquid equilibrium of CO_2 solubilization in water ($CO_2 + H_2O = H^+ + HCO_3^-$) can be readily perturbed by bubbling an inert as into the solution.[36] We try to recover the probe by bubbling nitrogen gas (N_2) to the CO_2-treated **1** solution. To our delight, the green fluorescence disappear after 2 min of N_2 bubbling, while the emission maximum was also restored to its initial state. This cycle could be repeated over 10 times without any considerable loss of sensing ability of the probe (Fig. 5c).

Logic behaviors of 1 with proton, CO_2 and amines as inputs

The PeT behavior, and consequently the fluorescence (output) properties, of **1** in the presence and absence of chemical input information can be interpreted within the framework of molecular logic. The output of OR gate is normally switched on if either one or both inputs are turned on.[37] As a consequence of observed fluorescence enhancement of **1** in the system of MeOH/H_2O in the presence of H^+ and CO_2, an OR gate can be easily applied by using H^+ and CO_2 as two chemical inputs and fluorescence as an output. In the absence of H^+ or CO_2, the fluorescence intensity of system **1** is relative low (output: 0) because of reductive PeT behavior, whereas the fluorescence intensities are obviously enhanced (output: 1) in the presence of each or both of the two inputs. As a result, a two-input OR logic gate is obtained according to the truth table in Fig. 6a.

Inhibit (INH) logic gates work basically as AND gates, where one of the input information is inverted through a NOT function.[37] INH logic deserves some attention because it demonstrates a noncommutative behavior; that is, one of the inputs can disable the whole system. The fluorescent intensity of CO_2-treated **1** solution was quenched upon the addition of amines. This system was found to be in agreement with the general formulation of an INH gate, wherein changes in CO_2 and amines concentration serve as the input and fluorescence intensity changes as the output (Fig. 6b).

(a)

In_1 (H^+)	In_2 (CO_2)	Out (λ_{em} 518 nm)
0	0	0
0	1	1
1	0	1
1	1	1

(b)

In_1 (CO_2)	In_2 (amines)	Out (λ_{em} 518 nm)
0	0	0
0	1	0
1	0	1
1	1	0

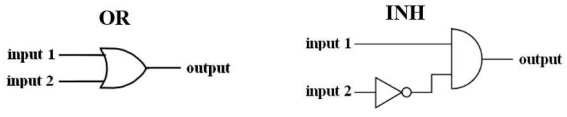

Fig 6 Truth table of the input-out relationships for two selected chemical inputs and equivalent combinatorial logic circuit for OR gate (a) and the Inhibit (INH) gate (b).

Conclusions

In this work, a simple aniline-substituted BODIPY derivative **1** behaves as a highly sensitive fluorescent probe. It shows more than 500-fold increase in fluorescent intensity within the pH range of 1.42 to 4.12 with a pK_a value of 3.24, which is valuable for use in strongly acidic environments. Besides, this probe was demonstrated as providing a convenient and easy-to-visualize fluorescent chemosensing system for the detection of dissolved CO_2 in the presence of water. Bubbling N_2 into the solution of CO_2-treated **1** can recover the sensing ability of the probe even if repeated for over 10 cycles. Furthermore, we have found that probe **1** can carry out multiple logic operations by selecting the initial states and chemical inputs. As a result, two logic gates (OR and INH) are achieved at the molecular level.

Acknowledgements

This work was supported by the National Natural Science Foundation of China (Grant Nos. 21201066 and 21203257), the Natural Science Foundation of Fujian Province (Grant No. 2011J01047), the outstanding Youth Scientific Research Cultivation Plan of Colleges and Universities of Fujian Province, and Promotion Program for Young and Middle-aged Teacher in Science and Technology Research of Huaqiao University (No. ZQN-PY104). Dr. Hai-Feng Su (Xiamen University) is greatly acknowledged for assistance with the ESI-MS experiments and we thank Dr. Hong-Xin Mei (Xiamen University) for help with the single-crystal X-ray diffraction data collections. Zhong-Hua Pan also thanks the National Innovative Foundation Project for undergraduates (No. 201310385004) for financial support.

References

(1) (a) R. G. Bates, *Chem. Rev.*, 1948, **42**, 1-61; (b) R. A. Gottlieb and A. Dosanjh, *Proc. Natl. Acad. Sci. U. S. A.*, 1996, **93**, 3587-3591; (c) K. Xu and A. M. Klibanov, *J. Am. Chem. Soc.*, 1996, **118**, 9815-9818.

(2) G. Mattock and G. R. Taylor, *pH Measurement and Titration*, Heywood, London, 1961, pp. 198-246.

(3) (a) J. Han and K. Burgess, *Chem. Rev.*, 2010, **110**, 2709-2728; (b) J. H. Lee, C. S. Lim, Y. S. Tian, J. H. Han and B. R. Cho, *J. Am. Chem. Soc.*, 2010, **132**, 1216-1217; (c) L. Yuan, W. Lin, Z. Cao, J. Wang and B. Chen, *Chem.-Eur. J.*, 2012, **18**, 1247-1255; (d) S. Madhu, M. R. Rao, M. S. Shaikh and M. Ravikanth, *Inorg. Chem.*, 2011, **50**, 4392-4400; (e) U. C. Saha, K. Dhara, B. Chattopadhyay, S. K. Mandal, S. Mondal, S. Sen, M. Mukherjee, S. V. Smaalen and P. Chattopadhyay, *Org. Lett.*, 2011, **13**, 4510-4513; (f) M. Baruah, W. W. Qin, N. Basarić, W. M. De Borggraeve and N. Boens, *J. Org. Chem.*, 2005, **70**, 4152-4157; (g) W. S. Zhang, B. Tang, X. Liu, Y. Y. Liu, K. H. Xu, J. P. Ma, L. L. Tong and G. W. Yang, *Analyst*, 2009, **134**, 367-371.

(4) The Molecuar Probes Handbook: A Guide to Fluorescent Probes and Labeling Technologies, ed. I. Johnson and M. T. Z. Spence, Invitrogen Corp., Carlsbad, 11th edn, 2010, pp. 894-897.

(5) M. Z. Tian, X. J. Peng, J. L. Fan, J. Y. Wang and S. Sun, *Dyes and Pigments*, 2012, **95**, 112-115.

(6) (a) R. N. Dansby-Sparks, J. Jin, S. J. Mechery, U. Sampathkumaran, T. W. Owen, B. D. Yu, K. Goswami, K. L. Hong, J. Grant and Z. L. Xue, *Anal. Chem.*, 2010, **82**, 593-600; (b) S. Neethirajan, D. S. Jayas and S. Sadistap, *Food Bioprocess. Tech.*, 2009, **2**, 115-121; (c) G. Eranna, B. C. Joshi, D. P. Runthala and R. P. Gupta, *Crit. Rev. Solid State*, 2004, **29**, 111-188.

(7) (a) S. Neethirajan, D. S. Jayas and S. Sadistap, *Food Bioprocess Technol.*, 2009, **2**, 115; (b) J. Lin, Trac-Trends *Anal. Chem.*, 2000, **19**, 541-552; (c) O. S. Wolfbeis, L. J. Weis, M. J. P. Leiner and W. E. Ziegler, *Anal. Chem.*, 1988, **60**, 2028-2030; (d) M. J. Hitchman and M. U. S. Park, Patent 6.365.022.2002.

(8) (a) C. S. Chu and Y. L. Lo, *Sens. Actuators, B* 2008, **129**, 120-125; (b) O. Oter, K. Ertekin and S. Derinkuyu, *Talanta*, 2008, **76**, 557-

563; (c) Y. Amao, N. Nakamura, *Sen. Actuators, B* 2005, **107**, 861-865.
(9) (a) R. Ali, T. Lang, S. M. Saleh, R. J. Meier, O. S. Wolfbeis, *Anal. Chem*., 2011, **83**, 2846-2851; (b) X. Xie, M. Pawlak, M. Tercier-Waeber and E. Bakker, *Anal. Chem.*, 2012, **84**, 3163-3169.
(10) (a) M. Ishida, K. Pyosang, C. Jiyoung, Y. Juyoung, K. Dongho and L. S. Jonathan, *Chem. Commun*., 2013, **49**, 6950-6952; (b) Z. Guo, N. R. Song, J. H. Moon, M. Kim, E. J. Jun, J. Choi, J. Y. Lee, C. W. Bielaski, J. L. Sessler and J. Yoon, *J. Am. Chem. Soc*., 2012, **134**, 17846-17849; (c) Y. Liu, Y. H. Tang, N. N. Barashkov, I. S. Irgibaeva, J. W. Y. Lam, R. R. Hu, D. Birimzhanova, Y. Yu and B. Z. Tang, *J. Am. Chem. Soc*., 2010, **132**, 13951-13953; (d) Q. Xu, S. Lee, Y. Cho, M. H. Kim, J. Bouffard and J. Yoon, *J. Am. Chem. Soc*., 2013, **135**, 17751-17754.
(11) (a) N. Boens, V. Leen and W. Dehaen, *Chem. Soc. Rev*., 2012, **41**, 1130; (b) A. Loudet and K. Burgess, *Chem. Rev*., 2007, **107**, 4891-4932; (c) G. Ulrich, R. Ziessel and A. Harriman, *Angew. Chem., Int. Ed*., 2008, **47**, 1184-1201.
(12) Y. C. Wang, D. K. Zhang, H. Zhou, J. L. Ding, Q. Chen, Y. Xiao and S. X. Qian, *J. Appl. Phys*., 2010, **108**, 033520.
(13) R. F. Kubin and A. N. Fletcher, *J. Lumin*., 1982, **27**, 455-462.
(14) A. Cui, X. Peng, J. Fan, X. Chen, Y. Wu and B. Guo, *J. Photochem. Photobiol. A* 2007, **186**, 85-92.
(15) M. Kollmannsberger, K. Rurack, U. Resch-Genger and J. Daub, *J. Phys. Chem. A* 1998, **102**, 10211-10220.
(16) (a) L. J. Henderson, *Am. J. Physiol.*, 1908, 21, 173-179; (b) K. A. Hasselbalch, *Biochem. Z*., 1917, 78, 112-144.
(17) T. Higashi, *ABSCOR*, Empirical Absorption Correction based on Fourier series Approximation; Rigaku Corporation: Tokyo, 1995.
(18) G. M. Sheldrick, *SHELXS-97*, Program for X-ray Crystal Structure Determination; University of Gottingen: Germany, 1997.
(19) G. M. Sheldrick, *SHELXL-97*, Program for X-ray Crystal Structure Refinement; University of Gottingen: Germany, 1997.
(20) L. J. Barbour, X-Seed, A software tool for Supramolecular Crystallography; *Supramol. Chem*. 2001, **1**, 189-191.
(21) A. L. Spek, Implemented as the *PLATON* Procedure, a Multi-purpose Crystallographic Tool; Utrecht University: Utrecht, The Netherlands, 1998.
(22) K. Brandenburg, *DIAMON*D, Version 3.1f; Crystal Impact GbR: Bonn, Germany, 2008.
(23) (a) M. A. Spackman, J. J. Mckinnon, *CrystEngComm* 2002, **4**, 378-392; (b) M. Spackman, D. Jayatilaka, *CrystEngComm* 2009, **11**, 19-32; (c) M. A. Spackman, J. J. Mckinnon, D. Jayatilaka, *CrystEngComm*., 2008, **10**, 377-388.
(24) F. H. Allen, O. Kennard, D. G. Watson, L. Brammer, A. G. Orpen, R. Taylor, *J. Chem. Soc., Perdin Trans. 2* 1987, S1-S19.
(25) M. J. Frisch, G. W. Trucks, H. B. Schlegel, G. E. Scuseria, M. A. Robb, J. R. Cheeseman, Jr. J. A. Montgomery, T. Vreven, K. N. Kudin, J. C. Burant, J. M. Millam, S. S.Iyengar, J. Tomasi, V. Barone, B. Mennucci, M. Cossi, G. Scalmani, N. Rega, G. A. Petersson, H. Nakatsuji, M. Hada, M. Ehara, K.Toyota, R. Fukuda, J. Hasegawwa, M. Ishida, T. Nakajima, Y. Honda, O. Kitao, H. Nakai, M. Klene, X. Li, J. E. Knox, H. P. Hratchian, J. B. Cross, V. Bakken, C. Adamo, J.Jaramillo, R. Gomperts, R. E. Dtratmann, O. Yazyev, A. J. Austin, R. Cammi, C. Pomelli, J. W. Ochterski, P. Y. Ayala, K. Morokuma, G. A. Voth, P. Salvador,J. J. Dannenberg, V. G. Zakrzewski, S. Dapprich, A. D. Daniels, M. C. Strain, O. Farkas, D. K. Malick, A. D. Rabuck, K. Raghavachari, J. B. Foresman, J. V. Ortiz, Q. Cui, A. G. Baboul, S. Clirrord, J. Cioslowski, B. B. Sterfanov, G. Liu, A. Liashenko, P. Piskorz, I. Komaromi, R. L. Martin, D. J. Fox, T. Keith, M. Al-Laham, C. Y. Peng, A. Nanayakkara, M. Challacombe, P. M. W. Gill, B. Hohnson, W. Chen, M. W. Wong, C. Gonzalez, J. A. Pople, *Gaussian 03, Revision E.01*, Gaussian, Inc., Wallingford, CT, 2004.
(26) (a) A. D. Becke, *Phys. Rev. A*, 1988, **38**, 3098-3100; (b) A. D. Becke, *J. Chem. Phys*., 1993, **98**, 1372-1377; (c) A. D. Becke, *J. Chem. Phys*., 1993, **98**, 5648-5652; (d) P. J. Stephens, F. J. Devlin, C. F. Chabalowski, M. J. Frisch, *J. Phys. Chem*., 1994, **98**, 11623-11627.
(27) C. Lee, W. Yang, R. G. Parr, *Phys. Rev. B*, 1988, **37**, 785-789.
(28) C. Peng, P. Y. Ayala, H. B. Schlegel, M. J. Frisch, *J. Comp. Chem*., 1996, **17**, 49.
(29) G. G. Luo, J. X. Xia, K. Fang, Q. H. Zhao, J. H. Wu and J. C. Dai, *Dalton Trans*., 2013, **42**, 16268-16271.
(30) Y. T. Chen, L. Wan, D. P. Zhang, Y. Z. Bian and J. Z. Jiang, *Photochem. Photobiol. Sci*., 2011, **10**, 1030-1038.
(31) (a) H. Lu, Z. L. Xue, J. Mack, Z. Shen, X. Z. You and N. Kobayashi, *Chem. Commun*., 2010, **46**, 3565-3567; (b) Y. T. Chen, H. L. Wang, L. Wan, Y. Z. Bian and J. Z. Jiang, *J. Org. Chem*., 2011, **76**, 3774-3781.
(32) D. Rehm, A. Weller, *Ber. Bunsenges. Phys. Chem*. **1969**, 73, 834-839.
(33) (a) M. Z. Tian, X. J. Peng, F. Feng, S. M. Meng, J. L. Fan, S. G. Sun, *Dyes and Pigments,* 2009, **81**, 58-62; (b) B. C. Guo, X. J. Peng, A. J. Cui, Y. K. Wu, M. Z. Tian, L. Z. Zhang, X. Q. Chen and Y. L. Gao, *Dyes and Pigments*, 2007, **73**, 206-210.
(34) A. Mills and G. A. Skinner, *Analyst*, 2010, **135**, 1912-1917.
(35) Y. Takagai, Y. Nojiri, T. Takase, W. L. Hinze, M. Butsugan and S. Igarashi, *Analyst*, 2010, **135**,1417-1425.
(36) Q. Yan, R. Zhou, C. Fu, H. Zhang, Y. Yin and J. Yuan, *Angew. Chem., Int. Ed*., 2011, **50**, 4923-4927.
(37) V. Balzani, M. Venturi, A. Credi, Molecular Devices and Machines: A Journey into the Nanoworld; Wiley-VCH: Weinheim, 2003.

Graphical Abstract

4-aniline BODIPY dye was developed as a highly sensitive fluorescent chemosensor for the detection of pH and CO_2 gas.